

Microstructure and photocatalytic activity of titanium dioxide nanoparticles*

Li Chun-Yan(李春艳)^{a)}, Wang Jiang-Bin(王江彬)^{b)}, and Wang Yi-Qian(王乙潜)^{a)†}

^{a)}*The Cultivation Base for State Key Laboratory, Qingdao University, Qingdao 266071, China*

^{b)}*Laiyang Zixilai Environmental Protection Technology Co. Ltd., North of Toll Station, Laiyang 265229, China*

(Received 13 January 2012; revised manuscript received 16 March 2012)

Titanium dioxide nanoparticles with an average diameter of about 10 nm are fabricated using a sintering method. The degradation of methyl orange indicates that the photocatalytic efficiency is greatly enhanced, which is measured to be 62.81%. The transmission electron microscopy is used to investigate the microstructure of TiO₂ nanoparticles in order to correlate with their photocatalytic properties. High-resolution transmission electron microscopy examinations show that all the nanoparticles belong to the anatase phase, and pure edge dislocations exist in some nanoparticles. The great enhancement of photocatalytic efficiency is attributed to two factors, the quantum size effect and the surface defects in the nanoparticles.

Keywords: titanium dioxide nanoparticles, high-resolution transmission electron microscopy, photocatalytic activity

PACS: 81.07.Bc, 68.37.Og, 84.60.Jt

DOI: 10.1088/1674-1056/21/9/098102

1. Introduction

In 1972, Fujishima and Honda^[1] discovered the photocatalytic splitting of water on titanium dioxide (TiO₂) electrode under the ultraviolet (UV) light. Since then, the TiO₂ material has attracted considerable attention due to its great potential for applications in catalysis,^[2] photocatalysis,^[3] and dye-sensitized solar cells.^[4,5] Especially, its high performance of degrading a wide range of both gaseous and aqueous contaminants is noted. In recent years, much effort has been devoted to obtaining TiO₂ nanomaterials with large surface areas and high photocatalytic activities, such as nanotubes, nanowires, nanoparticles (NPs), and thin films.^[6–10]

The TiO₂ nanomaterial has been frequently used in the field of photocatalysis due to its high efficiency, low-cost, non-toxicity, and light stability. However, there are still some limits to the catalytic activity of TiO₂, because it is active only under the UV light with an energy of more than 3.2 eV, and the photogenerated electrons and holes can easily recombine. More recently, much more work has been carried out to investigate the preparation and the catalytic properties

of TiO₂ NPs.^[4,11–13] The photocatalytic activity of TiO₂ NPs strongly depends on their microstructure. Extensive researches^[14–17] have shown that the sizes and the surface areas of TiO₂ particles can affect their photocatalytic activities. A lot of work^[18–20] has been conducted to improve the photocatalytic degradation efficiency by doping with other elements. However, doping techniques are complex, and few experimental studies are available concerning the relationship between their microstructure and photocatalytic activity.

In the present paper, we report on a detailed microstructure investigation of TiO₂ NPs fabricated by a simple sintering method. The degradation of methyl orange under the UV light is used to study their photocatalytic properties. The photocatalytic efficiency is greatly enhanced, and the reasons are explored.

2. Experiment

TiO₂ NPs were fabricated by using a simple sintering method. The reaction agent for the preparation was titanyl sulphate (TiOSO₄ · xH₂SO₄ · yH₂O). The raw materials were transported to the high temper-

*Project supported by the National Basic Research Program of China (Grant No. 2012CB722705), the Shandong Provincial Natural Science Foundation for Outstanding Young Scientists, China (Grant No. JQ201002), and the Shandong Provincial Scientific Research Award for Outstanding Young and Middle-Aged Scientists, China (Grant No. BS2009CL0005).

†Corresponding author. E-mail: yqwang@qdu.edu.cn

ature (600 °C) region with a material loading bowl. TiO₂ nanocrystals were obtained after sintering for 1 h, and the particles were exported through a cooling channel.

Specimens for TEM observations were prepared by dispersing the powder in alcohol by ultrasonic treatment for several minutes, and dropping onto a holey carbon film supported by a copper grid. High-resolution transmission electron microscopy (HRTEM) examinations were carried out using a JEOL JEM 2100F transmission electron microscope operating at 200 kV, whose point-to-point resolution was 2.4 Å.

A UV-757 spectrophotometer was used to measure the photocatalytic efficiency of the TiO₂ NPs. An aqueous solution of methyl orange (20 mg/L, 40 mL) was added to a solution of TiO₂ NPs (1.5 g/L). Then the mixture was divided into two parts. One part was stirred for 10 min by a magnetic stirrer, and the other was stirred under the UV light for 30 min. After centrifuging for 20 min at a rotation rate of 4000 r/min, clear liquids were separated, and then examined by the UV-757 spectrophotometer with the wavelength of 200–600 nm.

3. Results and discussion

Figure 1 shows a typical bright-field (BF) image of the TiO₂ NPs. From the figure, we can find two types of NPs, nearly spherical ones and elongated ones. To give a reliable prevalence distribution of the NPs, we record more than 200 NPs and carry out a statistical analysis of the particle type. The volume fraction of TiO₂ NPs with nearly spherical morphology

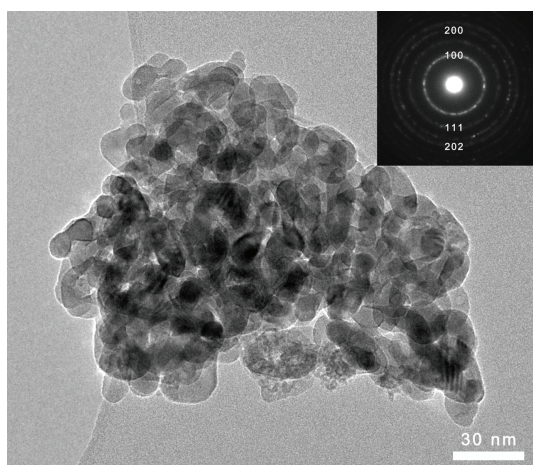


Fig. 1. Typical BF image of the TiO₂ NPs, and the inset shows the SAED pattern.

(~ 73.3%) is higher than that of NPs with elongated morphology (~ 26.7%). The TEM analysis of more than 200 NPs yields an average diameter of about 10 nm. The inset in Fig. 1 shows the corresponding selected area electron diffraction (SAED) pattern, which confirms that the particles are pure TiO₂ NPs. The diffraction rings are accord with the lattice parameters ($a = b \approx 3.78$ Å, $c \approx 9.52$ Å) of the anatase-phase TiO₂. The first four rings can be indexed as {100}, {111}, {200}, and {202}, respectively.

The degradation of methyl orange is used to evaluate the photocatalytic activity of the TiO₂ NPs. Figure 2 shows the absorbance of methyl orange with TiO₂ NPs versus the wavelength of the UV light. In Fig. 2, the solid curve is for the sample without the UV irradiation, and the dashed line is for the sample under the UV light irradiation. The absorbance peak of the sample under the UV light is much lower than that of the sample without the UV irradiation. The absorbance peak value of the sample without the UV irradiation is 2.388 at the wavelength of 501 nm, while that of the sample under the UV light is 0.888 at the wavelength of 493 nm. The photocatalytic efficiency η can be calculated from the peak value according to the following equation:

$$\eta = \frac{A_0 - A}{A_0} \times 100\%, \quad (1)$$

where A_0 and A are the absorbance peak values without and with the UV light for 30 min, respectively. Based on the experimental results, the photocatalytic efficiency is calculated to be 62.81%. The efficiency is twice higher than that reported by Bai *et al.*,^[21] Zhang *et al.*,^[22] and Yang *et al.*^[23] under the same experimental conditions. The photocatalytic efficiency increases about 20% compared with the results of Li *et al.*^[24]

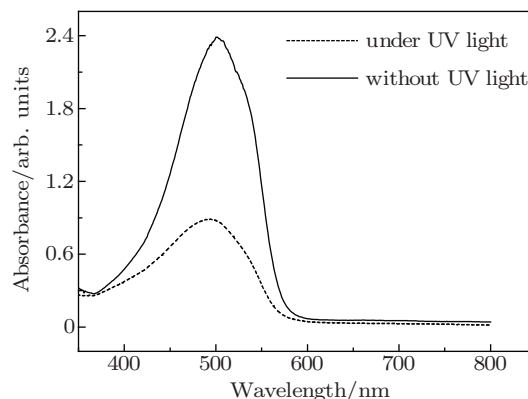


Fig. 2. UV-Vis spectra of methyl orange with TiO₂ NPs.

In order to clarify the mechanism under the great enhancement of photocatalytic efficiency, extensive

HRTEM examinations have been carried out. It is shown that spherical and elongated TiO₂ NPs coexist in the products. Figure 3 shows the typical HRTEM images of TiO₂ NPs. Figure 3(a) is a typical HRTEM image of nearly spherical NPs with an average diameter of about 6 nm, and figure 3(b) shows the enlarged HRTEM image of an individual nanoparticle. Figure 3(c) shows a typical HRTEM image of an elongated nanoparticle. From Fig. 3(c), it can be seen that the lattice fringes are of around 3.5 Å, corresponding to the {101} planes of the anatase phase. The HRTEM examination clearly shows that the nanoparticles belong to the anatase phase after sintering at 600 °C, similar to the results reported by Salari *et al.*^[25] Theoretical studies^[26,27] suggested that the surface energy of an anatase TiO₂ macroscopic crystal is smaller than that of the rutile phase. This could explain the fact that TiO₂ NPs prefer to possess the anatase structure. This is consistent with what we have observed from the HRTEM images.

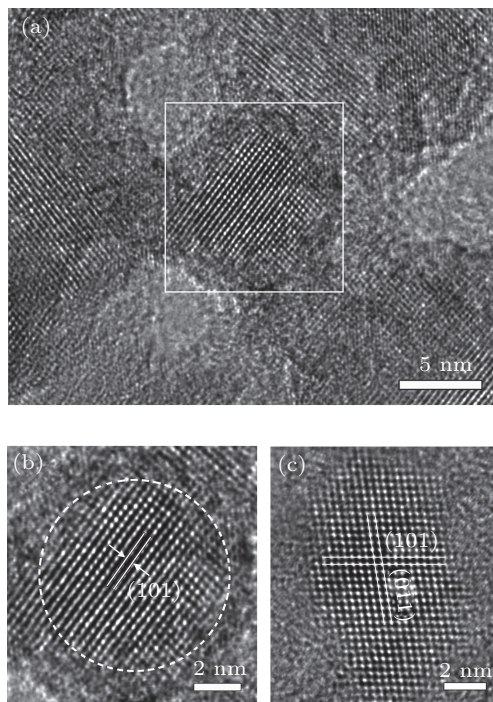


Fig. 3. HRTEM images of ((a), (b)) nearly spherical TiO₂ NPs and (c) the elongated TiO₂ NP.

Apart from the single crystalline NPs, TiO₂ NPs with defects have also been observed. Figure 4 is a HRTEM image of TiO₂ NPs showing a pure edge dislocation. The dislocation is indicated by D in Fig. 4(a). A characteristic of the perfect dislocation, the extra half atomic plane, is indicated by the dashed line in Fig. 4(a). An enlarged HRTEM image of the

dislocation is shown in Fig. 4(b), which shows the extra half atomic plane more clearly. The Burgers circuit for D is drawn to determine the Burgers vector, as shown in Fig. 4(c). From Fig. 4(c), it can be clearly seen that there is a gap between the starting and the ending points of the Burgers circuit, which is indicated by a white arrow. The Burgers vector for D is determined to be $\mathbf{b} = \langle \bar{1}21 \rangle$. The dislocations might be generated due to the existence of large strain in the sintering process.

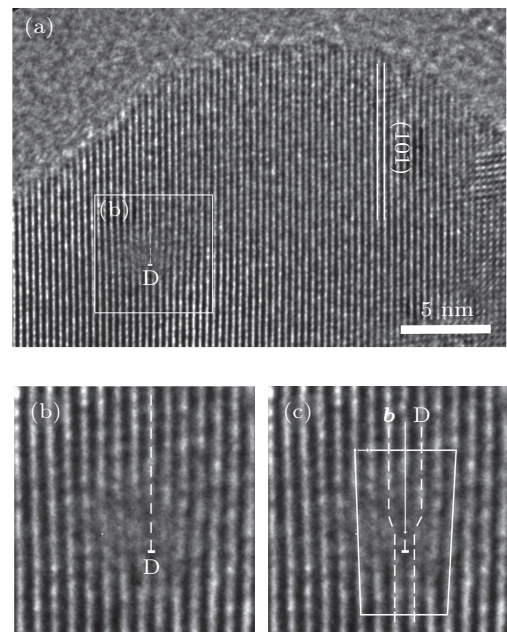
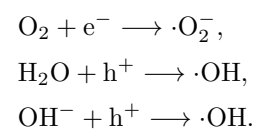


Fig. 4. (a) Typical HRTEM image of TiO₂ NPs with a dislocation structure; (b) enlarged HRTEM image showing the dislocation; (c) the Burgers circuit for dislocation D.

To correlate the microstructure with the higher efficiency, we first recall the mechanism of the photodegradation. In the photodegradation process, photoexcited electrons (e^-) are promoted from the valence band (VB) to the conduction band (CB), creating holes (h^+) at the VB edge as shown in Fig. 5. The photoexcited electrons and holes then are transferred to the surface of the particle and join the half-cell reactions. These electrons in the CB can form the $\cdot O_2^-$ with O_2 in a reduction process, while the holes in the VB can form the $\cdot OH$ with H_2O or OH^- in an oxidation process. The hydroxyl radicals react with the methyl orange and oxidize them into non-pollution products. The half-cell reactions are



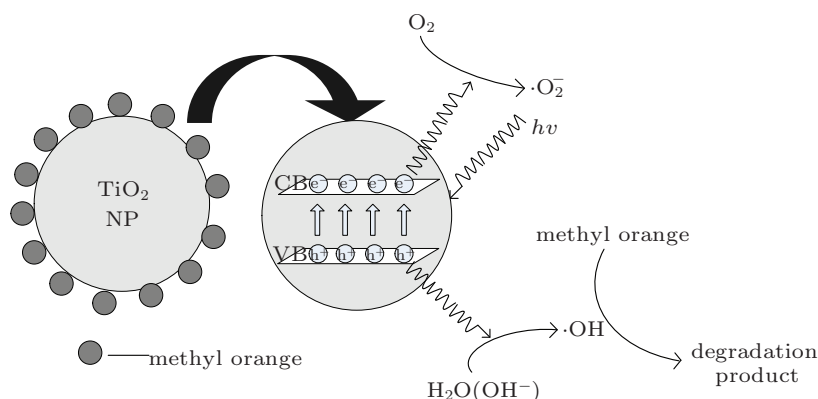


Fig. 5. Schematic diagram showing the photocatalytic activity of TiO₂ NPs.

Based on the photodegradation mechanism and the results of HRTEM investigation, the enhancement of photocatalytic degradation efficiency is ascribed to the small sizes and the surface defects of the TiO₂ NPs. On one hand, the TiO₂ NPs obtained in our experiment are small (~ 10 nm), so their surface areas increase a lot. The larger surface area will contribute to the preabsorption of O₂ and the degraded organics on the surfaces of the TiO₂ NPs, and thus a higher efficiency will be obtained. When the particle size is about 10 nm, a strong quantum size effect, which broadens the forbidden band, will appear. The broad forbidden band enhances the oxidation ability of the TiO₂ NPs, which will contribute to the great enhancement of the photocatalytic efficiency as well. In addition, there is a close relationship between the particle size and the time needed for the photogenerated electrons and holes to diffuse to the surface of particle. The relationship is shown by the following equation:

$$t = \frac{d^2}{k^2 D}, \quad (2)$$

where t is the time needed for the photogenerated electrons and holes to diffuse to the surface of the particle, D is the diffusion coefficient of the photogenerated electrons and holes, d is the diameter of the particle, and k is a constant. It can be clearly seen from Eq. (2) that t decreases as d reduces. So the recombination possibility for the photogenerated electrons and hole will be reduced, which results in a higher photocatalytic activity. On the other hand, dislocations exist in some anatase TiO₂ NPs. The dislocations usually terminate at the surfaces of NPs, which will cause more surface defects. It has been reported that surface defects such as stacking faults can enhance the photodegradation activity of TiO₂ NPs.^[28] Here, the

surfaces defects caused by the termination of dislocations on the surfaces of TiO₂ NPs act as active sites for the absorption of electron acceptors or donors, and thus the photocatalytic efficiency of the TiO₂ NPs is greatly enhanced.

4. Conclusion

In this work, TiO₂ NPs with an average diameter of about 10 nm are fabricated using a simple sintering method. The photocatalytic degradation of methyl orange is carried out to determine the photocatalytic efficiency of the TiO₂ NPs. The photocatalytic efficiency is about 62.81%, which is greatly enhanced. The great enhancement of photocatalytic efficiency is attributed to two factors, the quantum size effect and the surface defects in the NPs.

References

- [1] Fujishima A and Honda K 1972 *Nature* **238** 37
- [2] Hadjiivanov K I and Klissurski D G 1996 *Chem. Soc. Rev.* **25** 61
- [3] Linsebigler A L, Lu G Q and Yates J T 1995 *Chem. Rev.* **95** 735
- [4] Chen X B and Mao S S 1995 *Chem. Rev.* **107** 2891
- [5] Xu X Y, Hu L H, Li W X and Dai S Y 2011 *Acta Phys. Sin.* **60** 116802 (in Chinese)
- [6] Wang Y Q, Hu G Q, Duan X F, Sun H L and Xue Q K 2002 *Chem. Phys. Lett.* **365** 427
- [7] Hoyer P 1996 *Langmuir* **12** 1411
- [8] Shankar K, Basham J I, Allam N K, Varghese O K, Mor G K, Feng X J, Paulose M, Seabold J A, Choi K and Grimes C A 2009 *J. Phys. Chem. C* **113** 6327
- [9] Shi J W, Zheng J T and Wu P 2009 *J. Hazard. Mater.* **161** 416
- [10] Ding P, Liu F M, Yang X A and Li J Q 2011 *Acta Phys. Sin.* **60** 036803 (in Chinese)

- [11] Wang C C and Ying J Y 1999 *Chem. Mater.* **11** 3113
- [12] Billik P and Plesch G 2007 *Mater. Lett.* **61** 1183
- [13] Keswania R K, Ghodkea H, Sarkara D, Khilara K C and Srinivasa R S 2010 *Colloids Surf. A: Physicochem. Eng. Asp.* **369** 75
- [14] Anpo M, Shima T, Kodama S and Kubokawa Y 1987 *J. Phys. Chem.* **91** 4305
- [15] Zhang Z B, Wang C C, Zakaria R and Ying J Y 1998 *J. Phys. Chem. B* **102** 10871
- [16] Ruan S P, Wu F Q, Zhang T, Gao W, Xu B K and Zhao M Y 2001 *Mater. Chem. Phys.* **69** 7
- [17] Chen L X, Rajh T, Wang Z Y and Thurnauer M C 1997 *J. Phys. Chem. B* **101** 10688
- [18] Yang Y, Li X J, Chen J T and Wang L Y 2004 *J. Photochem. Photobiol. A: Chem.* **163** 517
- [19] Shevlin S A and Woodley S M 2010 *J. Phys. Chem. C* **114** 17333
- [20] Štengl V, Bakardjieva S and Murafa N 2009 *Mater. Chem. Phys.* **114** 217
- [21] Bai R, Li Q L, Zhang W, Li J Q and Hao Y 2010 *Technol. Dev. Chem. Ind.* **39** 3 (in Chinese)
- [22] Zhang L Y, Cao Y, Liu Z X, Yu X L and Lü Z F 2011 *Chin. J. Rare Metals* **35** 504 (in Chinese)
- [23] Yang H M, Zhang K, Shi R R, Li X W, Dong X D and Yu Y M 2006 *J. Alloys Compd.* **413** 302
- [24] Li Y J, Li X D, Li J W and Yin J 2005 *Catal. Commun.* **6** 650
- [25] Salari M, Mousavi Khoie S M, Marashi P and Rezaee M 2009 *J. Alloys Compd.* **469** 386
- [26] Lazzeri M, Vittadini A and Selloni A 2001 *Phys. Rev. B* **63** 155409
- [27] Oliver P M, Watson G W, Kelsey E T and Parker S C 1997 *J. Mater. Chem.* **7** 563
- [28] Choi H, Stathatos E and Dionysiou D D 2007 *Top. Catal.* **44** 513